PCCP

ROYAL SOCIETY OF CHEMISTRY

PAPER

View Article Online
View Journal | View Issue

Cite this: *Phys. Chem. Chem. Phys.*, 2024, **26**, 22252

Temperature-dependent structural dynamics in covalent organic frameworks observed by cryogenic infrared spectroscopy†

Silas O. Frimpong,[a] Nathan McLane,[b] Matthew Dietrich,[a] Garrison A. Bauer,[a] Michael R. Baptiste,[a] Leah G. Dodson *[a] and Mercedes K. Taylor *[a]

Understanding the structural dynamics of covalent organic frameworks (COFs) in response to external temperature change is necessary for these materials' application at cryogenic temperatures. Herein, we report reversible structural dynamics observed in covalent organic frameworks as the temperature varies from 298 K to 30 K. A series of frameworks (COF-300, COF-300-amine, and COF-V) was studied *in situ* using a cryogenic infrared spectroscopy system. We observed peak shifts in the Fourier-transform infrared (FTIR) spectrum of COFs as temperature cooled to 30 K, and these peak shifts were reversed as temperature returned to 298 K. Comparison of these materials showed different degrees of temperature-dependent change, through the quantitative degree of the peak shift and a qualitative description of which peaks shifted. A general IR peak shift towards a higher frequency as temperature decreased was observed, with COF-300 exhibiting quantitatively larger blue shifts in key vibrational modes as compared with the other frameworks. The nature of the conformational changes giving rise to the IR shifts was studied using quantum-chemistry calculations on model systems. The results of the calculations indicate that key peak shifts arise from a pedal motion experienced by the frameworks during cooling. This understanding of temperature-dependent framework dynamics will enhance the development, selection, and application of covalent organic frameworks at extreme temperatures.

Received 8th June 2024,
Accepted 4th August 2024

DOI: 10.1039/d4cp02338b

rsc.li/pccp

1. Introduction

Covalent organic frameworks (COFs) are porous materials constructed from organic building blocks, which covalently link in an orderly manner to form a crystalline framework.[1] These frameworks are characterized by their crystallinity,[1] tunability,[2] high surface area,[3] and stability,[3] a combination of properties that opens the door to diverse applications. Consequently, covalent organic frameworks have attracted research attention in the areas of catalysis,[4] energy storage,[5] sensors,[6,7] gas separation and storage,[8] metal capture,[9,10] and water purification.[11,12]

The emphasis on application has led covalent organic frameworks to be relentlessly functionalized and optimized, in a quest to design well-defined materials with industrial relevance.[13] In particular, increasing effort has been devoted to the design of structurally dynamic materials that respond reversibly to external stimuli.[14,15] The structural flexibility and enhanced stability of covalent organic frameworks allow them to undergo reversible transformations without decomposition, thereby maintaining the framework's integrity.[16] Conformational interconversions, including breathing, swelling, and linker rotation, are common features in covalent organic frameworks.[16–19]

External stimuli have also been shown to influence bond vibrations in these materials.[19–21] When temperature change is the external stimulus, frameworks have been found to undergo changes in lattice vibrations as well as changes in structure.[17,18] Other materials properties have been studied as a function of temperature using various spectroscopies, particularly using Raman spectroscopy.[22–25] However, few variable-temperature studies probe the framework behavior at cryogenic conditions, particularly at temperatures below 77 K.

This knowledge gap is important to address because of the promising cryogenic applications of covalent organic frameworks. In one recent example, Oh *et al.* explored the cryogenic flexibility of covalent organic frameworks for quantum sieving.[26] They were able to separate isotopes of hydrogen at cryogenic conditions due to a general contraction of the framework, which gave rise to

[a] *Department of Chemistry and Biochemistry, University of Maryland, College Park, Maryland 20742, USA. E-mail: mkt@umd.edu, ldodson@umd.edu*
[b] *Institute for Physical Science and Technology, University of Maryland, College Park, MD 20742, USA*

† Electronic supplementary information (ESI) available. See DOI: https://doi.org/10.1039/d4cp02338b

selectivity for hydrogen over deuterium. Hence, studying conformational changes under cryogenic conditions is crucial for the development of future applications, especially in adsorptive separations.

Fourier-transform infrared spectroscopy (FTIR) has recently been explored as a powerful technique to study framework behavior in response to external stimuli. Fang *et al.* conducted an *in situ* FTIR analysis to study the behavior of covalent organic frameworks in response to external pressure.[20] Upon applying pressure from 0 to 12 GPa, they observed a blue shift in most of the modes in the framework, with the C=N functional group experiencing the greatest effect. Because of the wealth of chemical information provided by FTIR spectroscopy, we used this technique to understand framework behavior at cryogenic temperatures.

We selected three well-known frameworks as representatives of three distinct structure types within the family of covalent organic frameworks (Fig. 1). The first, COF-300, is a framework with three-dimensional connectivity (3D COF) based on imine linkages.[27,28] The second framework, which we term COF-300-amine, is the amine-linked analog of COF-300.[29,30] The third framework, in contrast, is a two-dimensional material in which imine linkages connect monomers in two-dimensional planes; these 2D sheets are stacked through noncovalent interactions to yield a crystalline framework named COF-V.[31]

Using a novel FTIR spectroscopy system, we herein show that extremely low temperatures induce structural changes in these frameworks, encoded in changes in the IR spectra. Our cryogenic FTIR system was used to carry out an *in situ* structural study of these COFs at temperatures down to 30 K. Further comparison of these COFs revealed different degrees of change through the quantitative degree of the peak shift and a qualitative assignment of shifted peaks. Shifting peak positions in the IR spectra were identified using quantum-chemistry calculations to reveal the functional groups most impacted by cryogenic cooling. This is the first *in situ* study of the structural dynamics of covalent organic frameworks at cryogenic conditions as low as 30 K.

2. Experimental methods

2.1. Synthesis and characterization of covalent organic frameworks

We synthesized three known covalent organic frameworks for this study. Adapted from a previously reported solvothermal method,[27] COF-300 was synthesized by reacting tetrakis(4-aminophenyl)methane (TAPM; 1 eq.) and terephthaldehyde (2 eq.) in a solution of 1,4-dioxane and 6 M aqueous acetic acid. The mixture was degassed, sealed, and subjected to an elevated temperature of 120 °C for 72 hours. The synthesis of crystalline COF-300 was confirmed using powder X-ray diffraction (PXRD; see Fig. S4, ESI†).

Synthesis of COF-300-amine was carried out by the reduction of COF-300.[29] Treating imine-linked COF-300 with $NaBH_4$ (38 eq.) in anhydrous methanol at room temperature for 24 hours

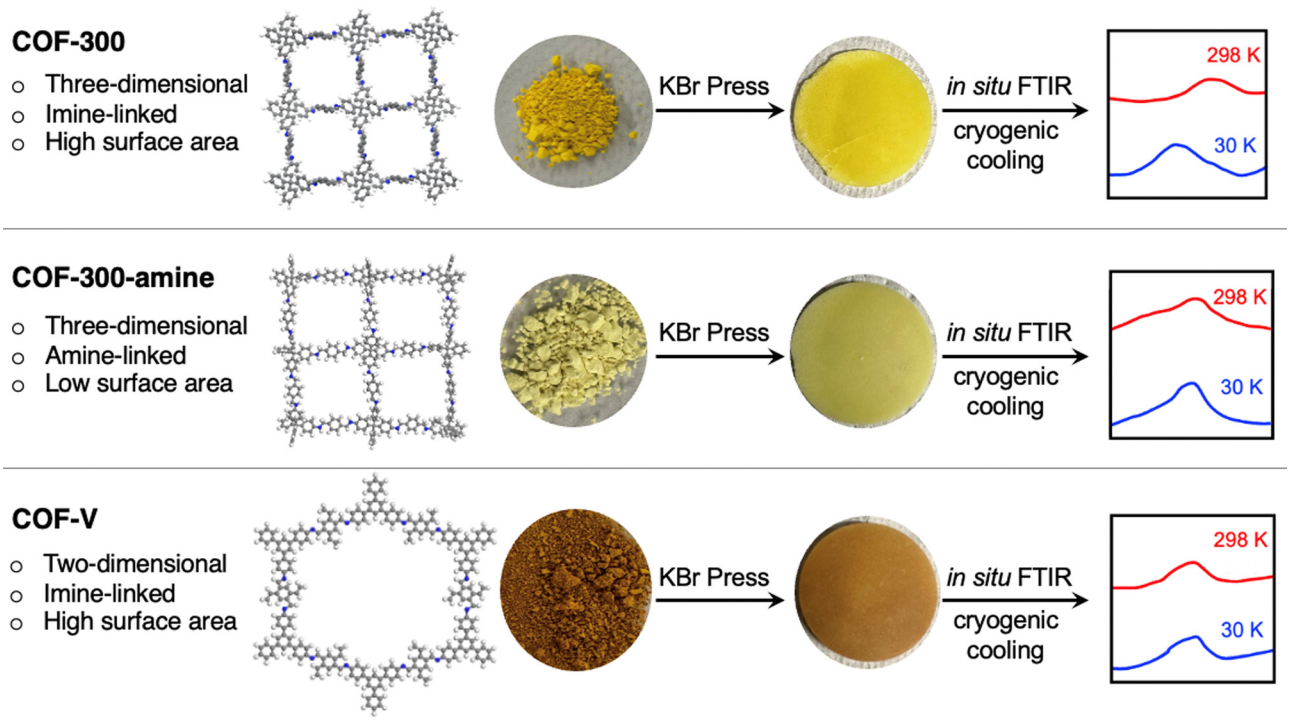

Fig. 1 Schematic depiction of the *in situ* FTIR analysis performed on three covalent organic frameworks. The image of the COF-300 structure was created from crystallographic data published in ref. 28; the images of the COF-300-amine and COF-V structures are simply illustrations created using the program Materials Studio.

in the presence of 1,4-benzenedicarboxylic acid (1 eq.) yielded amine-linked COF-300-amine. This was confirmed using solid-state ^{13}C cross-polarization magic-angle spinning NMR spectroscopy, which shows the disappearance of an imine carbon at 158 ppm and the appearance of amine carbon at 52 ppm in COF-300-amine (Fig. S1 and S2, ESI†).

The third framework, COF-V, was synthesized by combining 1,3,5-tris(4-aminophenyl)benzene (TPB) and 2,5-divinylterephthalaldehyde (DVA) in a solution of acetonitrile and 12 M acetic acid at room temperature for 72 h.[31] This afforded a brownish-yellow powder that was characterized by PXRD (Fig. S6, ESI†) and solid-state NMR (Fig. S3, ESI†). All covalent organic frameworks underwent extensive solvent exchanges and were vacuum-dried at 80 °C overnight before subsequent analysis.

2.2. Cryogenic FTIR experiment

2.2.1. Methodology. Measurement of low-temperature infrared spectra of the covalent organic frameworks was enabled by a new cryogenically cooled spectrometer designed and built by the Dodson group at the University of Maryland. The following sections describe this instrument in detail. Briefly, pressed pellets of an infrared-transparent matrix were doped with a small fraction of the covalent organic framework. The pellets were placed inside the FTIR sample chamber (described further below) and heated to 127 °C under vacuum (50 mTorr) for two hours, then cooled to room temperature while vacuum was maintained for two additional hours, to ensure complete evacuation of the pores. The pellets were then cooled to temperatures as low as 30 K inside a vacuum chamber, and the vibrational signatures of the covalent organic framework were monitored *via* FTIR spectroscopy as a function of temperature. The evolution of the framework structures as a function of temperature was interpreted based on assigning shifting vibrational modes through comparison to previous literature and to quantum-chemistry calculations.

2.2.2. Sample chamber. Porous material samples were isolated and cooled in a sample chamber that is based on a modified Advanced Research Systems model DMX-16SS closed-cycle helium cryostat system. A custom sample mount machined out of oxygen-free high thermal conductivity copper was mounted onto the second stage of the helium cryohead. The temperature of the sample was monitored with a DT-670B-SD silicon diode that is in physical contact with both the sample and its mount. Temperature control was achieved through a Lakeshore 336–3060 temperature controller that powers resistive heaters inserted into the sample mount, enabling temperatures to be maintained from 25–450 K. The pellet containing the covalent organic framework was positioned between the sample mount and an aluminum plate with a machined 0.75-inch diameter center hole. The plate was then screwed into the mount, allowing the sample pellet to be in direct contact with the sample stage. The cryostat cold head was encased by a vacuum shroud with custom optic ports housing ZnSe windows aligned collinear with the mounted sample pellet. The vacuum chamber was continuously pumped by an Agilent TriScroll 600 scroll pump to pressures as low as 50 mTorr without cryopumping, and 2.7 mTorr with cryopumping.

2.2.3. Infrared spectroscopy. Temperature-dependent infrared analysis on the covalent organic frameworks was conducted by positioning the sample chamber within the main compartment of a ThermoFisher iS50 Nicolet FTIR Spectrometer. A custom purge box was employed, surrounding the FTIR main compartment and the sample chamber, reducing background contributions from ambient gases in the resulting spectra. Infrared light produced by the FTIR instrument made a single pass, in ''transmission'' mode, through the sample arriving at a DTGS KBr detector. All spectra were obtained at a resolution of 1.0 cm^{-1} at a precision of 0.1 cm^{-1}, for a total of 75 scans.

2.2.4. Computational analysis. To interpret the observed infrared spectra and their temperature dependencies, we carried out quantum-chemistry calculations to simulate the vibrational spectra of model structures of the covalent organic frameworks. All calculations were carried out using Gaussian 16.[32]

Cluster models (Fig. S17, ESI†) were used to approximate the vibrational spectra of the extended frameworks and to assign observed peaks to specific functional groups. Geometries of the cluster models were optimized at the B3LYP level of theory including empirical dispersion (DFT-D3), using the cc-pVTZ basis.[33,34] Minimum structures were confirmed by the absence of imaginary frequencies, and the calculated harmonic vibrational frequencies were scaled by 0.968 to account for anharmonicities[35,36]

The effect of structural changes on vibrational spectra was simulated by carrying out relaxed geometry scans over the main dihedral angle in small molecules (*N*-benzylideneaniline and *N*-benzylaniline) that represent molecular fragments of COF-300 and COF-300-amine (Fig. S18, ESI†). The C–C═N–C dihedral angle was scanned in *N*-benzylideneaniline, and the C–C–N–C dihedral angle was scanned in *N*-benzylaniline. Each dihedral angle was scanned in +10° increments from the global minimum structure (defined as 0°) to a maximum of 20°. Geometries of the molecular fragments were reoptimized and harmonic frequencies were calculated at each point using B3LYP/6-311G++(d,p), including empirical dispersion (DFT-D3).

3. Results and discussion

A high-resolution cryogenic FTIR spectroscopic system was used to acquire low-temperature condensed-phase IR spectra of the covalent organic frameworks (Fig. 1). Samples were initially compressed at a pressure of 12 tons per $inch^2$ with KBr to form 1-inch diameter pellets with thicknesses ranging from 0.025–0.075 inches. To ensure that the preparation process did not cause a deformation of the frameworks, the samples were observed by IR and PXRD after compression at the same pressure, without KBr (Fig. S4–S6 and S19–S21, ESI†). The IR spectra and PXRD patterns are unchanged before and after compression, indicating that the preparation method did not cause any structural change to the frameworks.

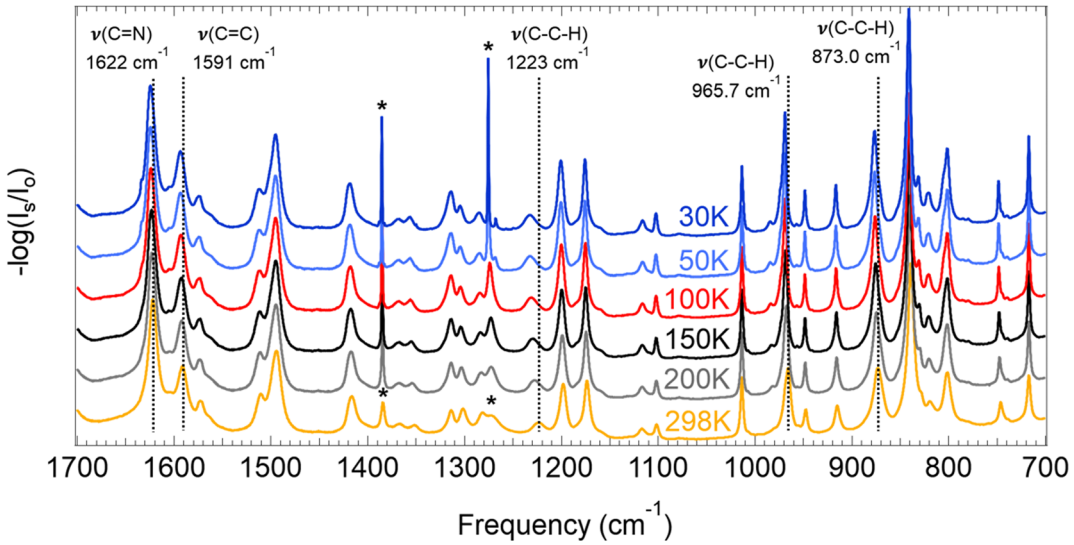

Fig. 2 FTIR spectra at varying temperatures for COF-300. Peaks marked with an asterisk are from H_2O and CO_2 contaminants in the KBr pellets and not from the samples under investigation. Spectra from 4000–700 cm^{-1} are given in Fig. S22 (ESI†).

The FTIR spectra of the covalent organic frameworks were then collected *in situ* at various temperatures from room temperature (measured to be 298 K) to as low as 30 K. As temperature decreased, we observed a gradual peak shift to higher frequency (shorter wavelengths) in most of the modes. This peak shift was shown to be reversible; when samples were then heated back to room temperature, the peaks returned to their original positions. Samples could be cycled repeatedly between 298 K and 30 K with no loss or change in peak shifting.

Of the three frameworks studied, COF-300 showed the greatest extent of peak shifting. While almost all peaks in the IR spectra (~30 peaks from 700 to 1700 cm^{-1}) were observed to shift by some amount in the COF-300 sample, we focus on assigning and describing five modes that are observed to shift by the greatest extent in COF-300 (without duplicating similar modes, *i.e.*, nearly-degenerate C=N stretches). Our peak assignments are given in Fig. 2, and an illustration of the regions of each mode is given in Fig. 3. Peak assignments came from the literature wherever possible, but peaks were assigned and confirmed based on our quantum chemistry calculations if no literature assignments were available. Peak shifts were quantified in two ways: (1) by evaluating the overall peak shift from room temperature to the lowest temperature (ν_{30K}–ν_{298K}), where a positive value indicates that a peak blue shifted when the sample became cold; and (2) by performing a linear fit of the peak centers observed as a function of temperature for all six temperatures used in these experiments, where slopes (cm^{-1} K^{-1}) that are negative indicate that the peak blue shifts as a function of decreasing temperature (Fig. 4).

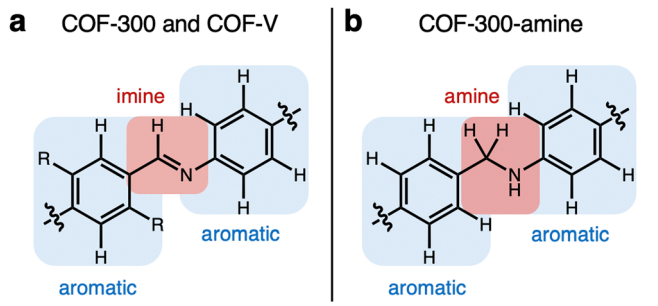

Fig. 3 Depiction of the functional groups containing the vibrational modes analyzed herein for COF-300 (a; R = H), COF-V (a; R = $CHCH_2$), and COF-300-amine (b).

For COF-300, the peak observed to undergo the greatest shift as a function of temperature is the C–C–H imine/aromatic stretch, centered at 1223.2 cm^{-1} at room temperature and shifting by 9.5 cm^{-1} to 1232.7 cm^{-1} at 30 K, with a slope of −0.038 cm^{-1} K^{-1}. The C–C–H bend (965.7 cm^{-1} at 298 K) shifts by about half as much, at a rate of −0.015 cm^{-1} K^{-1}, resulting in an overall ν_{30K}–ν_{298K} peak shift of 4.3 cm^{-1}. Another C–C–H bend appears at 873.0 cm^{-1} at 298 K and shifts at a slightly slower rate of −0.013 cm^{-1} K^{-1}, resulting in an overall ν_{30K}–ν_{298K} peak shift of 3.5 cm^{-1}. Two higher-energy peaks are observed to shift significantly in the COF-300 spectra. The first appears at 1621.9 cm^{-1} at room temperature and is assigned as the C=N imine stretch.[18,37,38] This peak shifts by 2.5 cm^{-1} at 30 K, at a rate of −0.0098 cm^{-1} K^{-1}. Finally, the peak assigned to the C=C aromatic stretch at 1591.3 cm^{-1} shifts by 2.2 cm^{-1} at 30 K, at a rate of −0.0081 cm^{-1} K^{-1}.

Similar modes in the COF-300-amine structure shift by smaller amounts—if at all (Fig. 5a). The peak that shifts by the largest amount in COF-300-amine is the C–N–H bend (1608.1 cm^{-1} at 298 K),[18,37,39] which blue shifts by 2.4 cm^{-1} at 30 K (−0.0093 cm^{-1} K^{-1}). Both C=C aromatic stretches shift by less than 2 cm^{-1}; at room temperature, the peaks appear at 1510.9 and 1461.5 cm^{-1}, and at 30 K they blue shift by 1.5 and 0.6 cm^{-1}, respectively (−0.0061 and −0.0017 cm^{-1} K^{-1}, respectively). The C–C–H bend vibration (1184.8 cm^{-1} at 298 K) also shifts by a small observable amount (ν_{30K}–ν_{298K} = 0.4 cm^{-1},

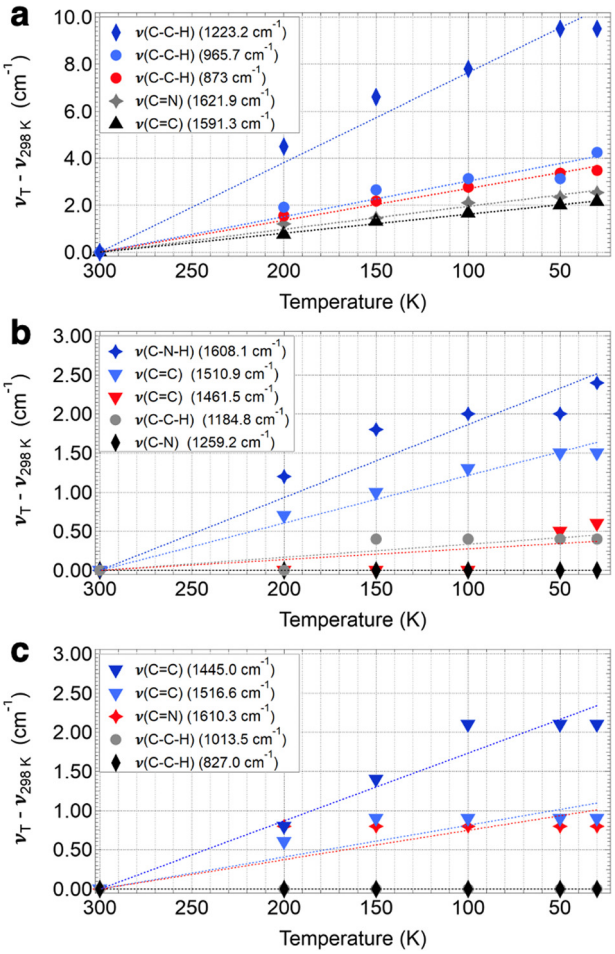

Fig. 4 Peak shifts as a function of temperature for COF-300 (a), COF-300-amine (b), and COF-V (c). Symbols are the peak shift for each temperature T and dotted lines are the linear fit for the temperature dependence of the shift for each mode, which was constrained to intersect 0 cm^{-1} at room temperature.

-0.0014 cm^{-1} K^{-1}). A distinguishing vibrational mode in COF-300-amine is the C–N stretch of the amine linkage (1259.2 cm^{-1}),[18,37,39] a functional group which is not present in COF-300; this mode is notably not observed to shift as a function of temperature. This observation agrees with the work of Chi *et al.*, who found that the mode near 1252 cm^{-1} within COF-300-amine is invariant under temperatures ranging from 300 K up to 500 K.[18]

The two-dimensional COF-V had even less quantitative peak shifting observed as a function of temperature (Fig. 5b). The two aromatic C=C stretches blue shift by 2.1 and 0.9 cm^{-1} (from 1445.0 and 1516.6 cm^{-1}, respectively, at 298 K) at a rate of -0.0087 and -0.0041 cm^{-1} K^{-1}, respectively. The room-temperature C=N stretch at 1610.3 cm^{-1} shifts by a small amount ($\nu_{30K}-\nu_{298K}$ = 0.8 cm^{-1}, -0.0037 cm^{-1} K^{-1}).[40] Both C–C–H bend vibrations at 1013.5 and 827.0 cm^{-1} remain unshifted as a function of temperature. Peak assignments for the selected vibrational modes discussed above are given in Table 1.

Overall, the three-dimensional, imine-linked framework COF-300 showed a greater average blue shift than its amine-linked counterpart COF-300-amine and the two-dimensional framework COF-V. This increase in vibrational frequency in COF-300 could be partly attributed to "pedal motion" experienced by the framework in response to an external stimulus.[17,18] Pedal motion has been observed in organic crystals such as stilbenes, azobenzenes, and benzylideneanilines with C=C, N=N or C=N functionalities.[17,18,41] In the pedal analogy, phenyl rings act as the pedals of a bicycle while the central double bond acts as the crank arm (Fig. 6a and b). Such pedal motion has been reported to cause a conformational interconversion of organic crystals as a function of temperature.[18] Hence, changes in the vibrational frequencies as temperature decreases may indicate conformational change in the pedal motif of COF-300. We note that this pedal motion is likely to occur in tandem with other structural changes throughout the framework, as has been observed for other covalent organic frameworks in response to external stimuli.[20]

The assigned experimental spectra show that the functional groups involved in the pedal motion in COF-300 are the most impacted by temperature change. To better understand this observation, we used quantum-chemistry calculations to explore the effect of the pedal motion on IR peak position *in silico*. We varied the dihedral angle between the planes of the two "pedals," or phenyl rings; the energy-optimized ground-state configuration was defined as an angle of 0° (Fig. 6c and d). Fig. 7a shows a portion of the simulated vibrational spectrum for *N*-benzylideneaniline (a molecular fragment of COF-300 containing the pedal motif) at three different dihedral angles. (The full spectra are plotted in Fig. S14 and S15 (ESI†), and all vibrational frequencies and shifts are in Tables S1 and S2. Line widths were set to 11.7 cm^{-1} for comparison to experimental spectra). Most of the vibrational modes red shift as a function of increasing dihedral angle, including the C=N stretch, which red shifts by more than 11.5 cm^{-1} as the angle increases from 0° to 20°. When considered in the context of the IR spectra discussed above, we interpret this *in silico* result to mean that the COF-300 pedal motif exhibits greater dihedral angles at room temperature than at 30 K. As the sample cools to 30 K, the dihedral angle decreases, resulting in a blue shift in the observed vibrational frequencies. Looking macroscopically at the larger framework, this rotation will lead to not only a variation in the frequency in the C=N mode but different interactions arising from the rotation of the attached crank arms, thus affecting other vibrational modes.

In comparison, a fragment of COF-300-amine containing the pedal motif (*N*-benzylaniline) shows only a slight red shift in the calculated C–N–H bend but substantial shifting among the other calculated peaks, as the dihedral angle increases from 0° to 20° (Fig. 7b and Fig. S15, Table S2, ESI†). This *in silico* result is in contrast with our experimental spectra, which show that the C–N–H bend shifts by the greatest amount, with other modes affected in only minor ways. These observations imply that the pedal motion is likely not driving any structural change that may occur in COF-300-amine as a function of temperature, consistent with the high-temperature results reported by Chi *et al.* for this framework.[21]

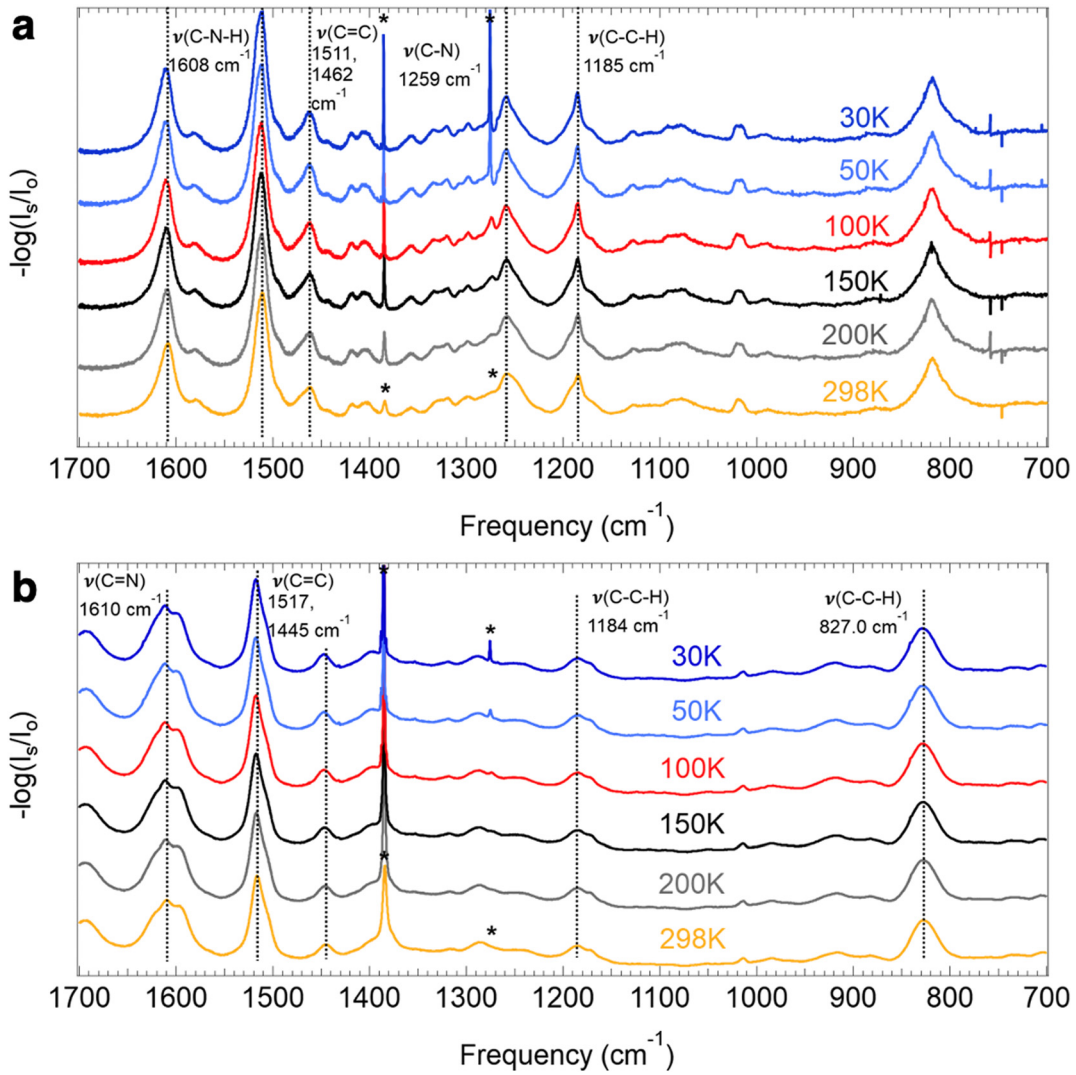

Fig. 5 FTIR spectra at varying temperatures for COF-300-amine (a) and COF-V (b). Peaks marked with an asterisk are from H_2O and CO_2 contaminants in the pellets and not from the samples under investigation. Spectra from 4000–700 cm^{-1} are given in Fig. S23 and S24 (ESI†).

The relative lack of pedal motion in COF-300-amine may appear counterintuitive, since the sp^3-hybridized atoms in its amine linkage are expected to allow for greater rotation and bond flexibility than the sp^2-hybridized atoms in the COF-300 imine linkage. We hypothesize that this bond flexibility allows COF-300-amine to adopt a contracted structure under vacuum; such a contracted structure is stabilized by intra-framework interactions and resistant to temperature-induced structural change. In addition to our IR spectroscopy results, our gas adsorption results also support this hypothesis. The N_2 sorption isotherm taken at 77 K shows a drastic decrease in adsorption capacity for COF-300-amine compared to COF-300 (Fig. S7, ESI†); the Brunauer–Emmett–Teller (BET) surface area measured for COF-300 reduced from 1383 $m^2\ g^{-1}$ to 13 $m^2\ g^{-1}$ in COF-300-amine. Literature reports also support the low N_2 uptake of COF-300-amine[37,39] and of other frameworks with freely-rotating linkages.[42,43] This large loss in surface area is not accompanied by framework degradation, as shown by PXRD and SEM (Fig. S5 and S9, ESI†). Thus, a structural contraction under vacuum that prevents N_2 from entering the pores of COF-300-amine may explain the framework's low BET surface area as well as its resistance to temperature-induced pedal motion.

Since the two-dimensional framework COF-V contains the same imine-linked pedal motif as COF-300, it would be reasonable to assume that structural changes driven by pedal motion should occur as the COF-V sample is cooled to cryogenic temperatures. However, our experimental results show little change in the observed spectra as a function of temperature. The defining aspect of two-dimensional covalent organic frameworks is their flat, sheet-like nature stacked together by π–π interactions. The tight packing of these sheets greatly inhibits their structural flexibility along the *z*-dimension (perpendicular to the planes of the sheets).[19] Consequently, changes in dihedral angle associated with pedal motion are hindered by the close inter-layer stacking of two-dimensional frameworks, which likely explains the minor extent of peak shifting we observed experimentally for COF-V.

Table 1 Peak centers (cm^{-1}) as a function of temperature for selected vibrational modes of COF-300, COF-300-amine, and COF-V, with the change in wavenumber ($\nu_{30K}-\nu_{300K}$) for these modes. The slope (cm^{-1} K^{-1}) obtained from a linear fit across all temperatures is also reported

298 K	200 K	150 K	100 K	50 K	30 K	$\nu_{30K}-\nu_{300K}$	Slope	Mode
COF-300								
1621.9	1623.1	1623.4	1624.0	1624.3	1624.4	2.5	−0.098	C═N imine stretch
1591.3	1592.0	1592.6	1592.9	1593.3	1593.4	2.2	−0.0081	C═C aromatic stretch
1223.2	1227.7	1229.8	1231.0	1232.7	1232.7	9.5	−0.038	C–C–H imine/aromatic stretch
965.7	967.6	968.4	968.8	968.8	970.0	4.3	−0.015	C–C–H bend
873.0	874.6	875.2	875.8	876.4	876.5	3.5	−0.013	C–C–H bend
COF-300-amine								
1608.1	1609.3	1609.9	1610.1	1610.1	1610.5	2.4	−0.0093	C–N–H bend
1510.9	1511.6	1511.9	1512.2	1512.4	1512.4	1.5	−0.0061	C═C aromatic stretch
1461.5	1461.5	1461.5	1461.5	1462.0	1462.1	0.6	−0.0017	C═C aromatic stretch
1259.2	1259.2	1259.2	1259.2	1259.2	1259.2	0.0	0.0	C–N stretch
1184.8	1184.8	1185.2	1185.2	1185.2	1185.2	0.4	0.0014	C–C–H bend
COF-V								
1610.3	1611.1	1611.1	1611.1	1611.1	1611.1	0.8	−0.0037	C═N stretch
1516.6	1517.2	1517.5	1517.5	1517.5	1517.5	0.9	−0.0041	C═C aromatic stretch
1445.0	1445.8	1446.4	1447.1	1447.1	1447.1	2.1	−0.0087	C═C aromatic stretch
1013.5	1013.5	1013.5	1013.5	1013.5	1013.5	0.0	0.0	C–C–H bend
827.0	827.0	827.0	827.0	827.0	827.0	0.0	0.0	C–C–H bend

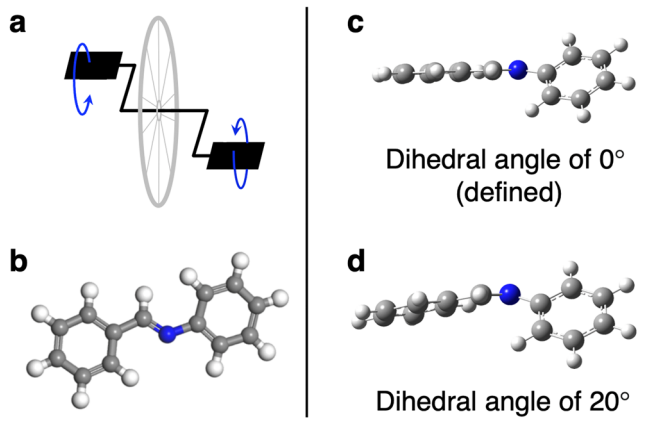

Fig. 6 Illustration of the pedal analogy (a) for motion around the C═N functionality in *N*-benzylideneaniline (b). Depiction of varying dihedral angle in *N*-benzylideneaniline, from the ground-state configuration (c) to an angle of 20° (d).

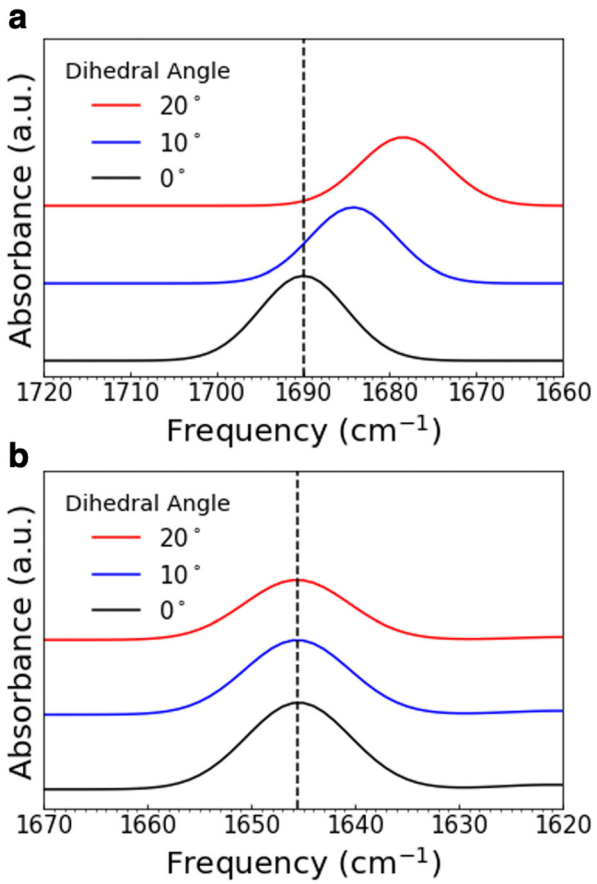

Fig. 7 Simulated IR peaks for varying dihedral angles in *N*-benzylideneaniline (a) and *N*-benzylaniline (b). Shown are just a portion of the spectrum; the C═N stretch in (a) and the C–N–H bend in (b).

Overall, our results show that the cooling-induced conformational changes are enhanced for COF-300, reduced for COF-300-amine, and minimized for COF-V. In comparing the design elements of the three frameworks, we note several distinctions: three-dimensional *vs.* two-dimensional connectivity, high *vs.* low BET surface area, and imine linkages with rigid sp^2 character *vs.* amine linkages with flexible sp^3 character. The interplay between these structural elements determines whether or not a framework experiences major conformational transformations in response to cryogenic cooling. These results can inform the selection of a given framework for cryogenic applications and can guide synthetic chemists in the design of new frameworks that show temperature-dependent behavior.

4. Conclusions

A series of covalent organic frameworks were subjected to cryogenic temperatures as a form of external stimulus. We studied the conformational transformations in these materials by observing the infrared spectra *in situ* during the cooling process. We observed a greater overall blue shift in the IR spectrum of the three-dimensional, imine-linked framework COF-300, compared to amine-linked COF-300-amine and two-dimensional COF-V.

We attribute these observations to the combination of high BET surface area with significant pedal motion about the C=N linkages in COF-300. This combination of structural features allows for greater conformational change as COF-300 cools, compared to the frameworks with low surface area or inhibited pedal motion. We conducted quantum-chemistry calculations on molecular fragments of the covalent organic frameworks to probe how IR peak positions change in response to pedal motion in these fragments. This work provides insight into the structural features of covalent organic frameworks that give rise to temperature-dependent IR shifts. Relationships between framework structure and response to cooling can guide future efforts to apply covalent organic frameworks to cryogenic applications, which are particularly relevant for gas storage and separations.

Data availability

The data supporting this article have been included as part of the ESI.† All electronic structure and frequency analysis output files can be accessed *via* FigShare, DOI: **10.6084/m9.figshare.26510275.v1**.

Conflicts of interest

There are no conflicts to declare.

Acknowledgements

We thank the University of Maryland, College Park for funding. We also thank the National Science Foundation (NSF-1726058) for funding a solid-state NMR spectrometer. We acknowledge the support of the Maryland NanoCenter and its AIMLab and the University of Maryland supercomputing resources (**https://hpcc.umd.edu**) made available for conducting the research reported in this paper. M. K. T. acknowledges funding from the Gordon and Betty Moore Foundation through award #12070. L. G. D. acknowledges that this material is based upon work supported by the U. S. Department of Energy, Office of Science Early Career Research Program, Office of Basic Energy Sciences under Award Number DE-SC0024262.

References

1 A. P. Cote, *Science*, 2005, **310**, 1166–1170.
2 N. Sinha and Srimanta Pakhira, *ACS Appl. Electron. Mater.*, 2021, **3**, 720–732.
3 T. Ben, H. Ren, S. Ma, D. Cao, J. Lan, X. Jing, W. Wang, J. Xu, F. Deng, J. M. Simmons, S. Qiu and G. Zhu, *Angew. Chem., Int. Ed.*, 2009, **48**, 9457–9460.
4 Z. Zhao, Y. Zheng, C. Wang, S. Zhang, J. Song, Y. Li, S. Ma, P. Cheng, Z. Zhang and Y. Chen, *ACS Catal.*, 2021, **11**, 2098–2107.
5 Y. Yusran, H. Li, X. Guan, D. Li, L. Tang, M. Xue, Z. Zhuang, Y. Yan, V. Valtchev, S. Qiu and Q. Fang, *Adv. Mater.*, 2020, **32**, 1907289.
6 Y. Sun, G. I. N. Waterhouse, L. Xu, X. Qiao and Z. Xu, *Sens. Actuators, B*, 2020, **321**, 128501.
7 E. Martinez-Perinan, M. Martínez-Fernández, J. L. Segura and E. Lorenzo, *Sensors*, 2022, **22**, 4758.
8 J. M. Vicent-Luna, A. Luna-Triguero and S. Calero, *J. Phys. Chem. C*, 2016, **120**, 23756–23762.
9 N. A. Babujohn, A. Eluri and V. P. Nabeela, *Chem. Eng. J.*, 2023, **464**, 142459.
10 A. Modak, P. Bhanja, M. Selvaraj and A. Bhaumik, *Environ. Sci. Nano*, 2020, **7**, 2887–2923.
11 S. Kandambeth, B. P. Biswal, H. D. Chaudhari, K. C. Rout, S. H. Kunjattu, S. Mitra, S. Karak, A. Das, R. Mukherjee, U. K. Kharul and R. Banerjee, *Adv. Mater.*, 2016, **29**, 1603945.
12 Y. Song, J. Phipps, C. Zhu and S. Ma, *Angew. Chem., Int. Ed.*, 2023, **135**, e202216724.
13 P. J. Waller, F. Gándara and O. M. Yaghi, *Acc. Chem. Res.*, 2015, **48**, 3053–3063.
14 Y. Yang, A. P. Sandra, A. Idström, C. Schäfer, M. Andersson, L. Evenäs and K. Börjesson, *J. Am. Chem. Soc.*, 2022, **144**, 16093–16100.
15 Y. Wang, M. S. Shim, N. S. Levinson, H.-W. Sung and Y. Xia, *Adv. Funct. Mater.*, 2014, **24**, 4206–4220.
16 Z.-B. Zhou, H.-H. Sun, Q.-Y. Qi and X. Zhao, *Angew. Chem., Int. Ed.*, 2023, **135**, e202305131.
17 J. Harada and K. Ogawa, *Chem. Soc. Rev.*, 2009, **38**, 2244.
18 H. Chi, Y. Liu, Z. Li, W. Chen and Y. He, *Nat. Commun.*, 2023, **14**, 5061.
19 C. Ji, C. Kang, B. Chandra Patra and D. Zhao, *CCS Chem.*, 2023, 1–26.
20 J. Fang, Z. Fu, X. Chen, Y. Liu, F. Chen, Y. Wang, H. Li, Y. Yusran, K. Wang, V. Valtchev, S. Qiu, B. Zou and Q. Fang, *Angew. Chem.*, DOI: **10.1002/anie.202304234**.
21 Y. Chen, Z.-L. Shi, L. Wei, B. Zhou, J. Tan, H.-L. Zhou and Y.-B. Zhang, *J. Am. Chem. Soc.*, 2019, **141**, 3298–3303.
22 R. Yan, J. R. Simpson, S. Bertolazzi, J. Brivio, M. Watson, X. Wu, A. Kis, T. Luo, A. R. Hight Walker and H. G. Xing, *ACS Nano*, 2014, **8**, 986–993.
23 H. M. Hill, A. F. Rigosi, S. Krylyuk, J. Tian, N. V. Nguyen, A. V. Davydov, D. B. Newell and A. R. Hight, *Phys. Rev. B*, 2018, **98**, 165109.
24 A. McCreary, J. R. Simpson, T. T. Mai, R. D. McMichael, J. E. Douglas, N. Butch, C. Dennis, R. Valdés Aguilar and A. R. Hight, *Phys. Rev. B*, 2020, **101**, 064416.
25 H. Iturriaga, L. M. Martinez, T. T. Mai, A. J. Biacchi, M. Augustin, A. R. Hight Walker, M. Fathi Sanad, S. T. Sreenivasan, Y. Liu, E. J. G. Santos, C. Petrovic and S. R. Singamaneni, *npj 2D Mater. Appl.*, 2023, **7**, 56.
26 H. Oh, S. Babu Kalidindi, Y. Um, S. Bureekaew, R. Schmid, R. A. Fischer and M. Hirscher, *Angew. Chem., Int. Ed.*, 2013, **52**, 13219–13222.
27 F. J. Uribe-Romo, J. R. Hunt, H. Furukawa, C. Klöck, M. O'Keeffe and O. M. Yaghi, *J. Am. Chem. Soc.*, 2009, **131**, 4570–4571.

28 T. Ma, E. A. Kapustin, S. X. Yin, L. Liang, Z. Zhou, J. Niu, L.-H. Li, Y. Wang, J. Su, J. Li, X. Wang, W. D. Wang, W. Wang, J. Sun and O. M. Yaghi, *Science*, 2018, **361**, 48–52.
29 H. Liu, J. Chu, Z. Yin, X. Cai, L. Zhuang and H. Deng, *Chem*, 2018, **4**, 1696–1709.
30 A. N. Zeppuhar, D. S. Rollins, D. L. Huber, E. A. Bazan-Bergamino, F. Chen, H. A. Evans and M. K. Taylor, *ACS Appl. Mater. Interfaces*, 2023, **15**, 52622–52630.
31 W. Ma, Q. Zheng, Y. He, G. Li, W. Guo, Z. Lin and L. Zhang, *J. Am. Chem. Soc.*, 2019, **141**, 18271–18277.
32 I. Gaussian, *Gaussian 16 IOps Manual*, 2016.
33 P. Carbonniere, T. Lucca, C. Pouchan, N. Rega and V. Barone, *J. Comput. Chem.*, 2005, **26**, 384–388.
34 S. Grimme, J. Antony, S. Ehrlich and H. Krieg, *J. Chem. Phys.*, 2010, **132**, 154104.
35 P. Sinha, S. E. Boesch, C. Gu, R. A. Wheeler and A. K. Wilson, *J. Phys. Chem. A*, 2004, **108**, 9213–9217.
36 J. P. Merrick, D. Moran and L. Radom, *J. Phys. Chem. A*, 2007, **111**, 11683–11700.
37 P. Jin, X. Niu, F. Zhang, K. Dong, H. Dai, H. Zhang, W. Wang, H. Chen and X. Chen, *ACS Appl. Mater. Interfaces*, 2020, **12**, 20414–20422.
38 Z. Wang, Z. Si, D. Cai, L. Shufeng and P. Qin, *J. Membr. Sci.*, 2020, **615**, 118466.
39 M. Kong, P. Jin, W. Wei, W. Wang, H. Qin, H. Chen and J. He, *Microchem. J.*, 2021, **160**, 105650.
40 Q. Jiang, Y. Li, X. Zhao, P. Xiong, X. Yu, Y. Xu and L. Chen, *J. Mater. Chem. A*, 2018, **6**, 17977–17981.
41 J. Harada, M. Harakawa and K. Ogawa, *Acta Crystallogr. Sect. B, Struct. Sci.*, 2004, **60**, 589–597.
42 X. Liu, J. Li, B. Gui, G. Lin, Q. Fu, S. Yin, X. Liu, J. Sun and C. Wang, *J. Am. Chem. Soc.*, 2021, **143**, 2123–2129.
43 X. Liu, Z. Wang, Y. Zhang, N. Yang, B. Gui, J. Sun and C. Wang, *J. Am. Chem. Soc.*, 2024, **146**, 11411–11417.

